Inflammatory signals from photoreceptor modulate pathological retinal angiogenesis via c-Fos

Ye Sun,[1] Zhiqiang Lin,[2] Chi-Hsiu Liu,[1] Yan Gong,[1] Raffael Liegl,[1] Thomas W. Fredrick,[1] Steven S. Meng,[1] Samuel B. Burnim,[1] Zhongxiao Wang,[1] James D. Akula,[1] William T. Pu,[2,3] Jing Chen,[1] and Lois E.H. Smith[1]

[1]Department of Ophthalmology and [2]Department of Cardiology, Harvard Medical School, Boston Children's Hospital, Boston, MA 02115
[3]Harvard Stem Cell Institute, Harvard University, Cambridge, MA 02138

Pathological neovessels growing into the normally avascular photoreceptors cause vision loss in many eye diseases, such as age-related macular degeneration and macular telangiectasia. Ocular neovascularization is strongly associated with inflammation, but the source of inflammatory signals and the mechanisms by which these signals regulate the disruption of avascular privilege in photoreceptors are unknown. In this study, we found that c-Fos, a master inflammatory regulator, was increased in photoreceptors in a model of pathological blood vessels invading photoreceptors: the very low-density lipoprotein receptor–deficient ($Vldlr^{-/-}$) mouse. Increased c-Fos induced inflammatory cytokines interleukin 6 (IL-6) and tumor necrosis factor (TNF), leading to activation of signal transducer and activator of transcription 3 (STAT3) and increased TNFα–induced protein 3 (TNFAIP3) in $Vldlr^{-/-}$ photoreceptors. IL-6 activated the STAT3/vascular endothelial growth factor A (VEGFA) pathway directly, and elevated TNFAIP3 suppressed SOCS3 (suppressor of cytokine signaling 3)–activated STAT3/VEGFA indirectly. Inhibition of c-Fos using photoreceptor-specific AAV (adeno-associated virus)-hRK (human rhodopsin kinase)–sh_c-fos or a chemical inhibitor substantially reduced the pathological neovascularization and rescued visual function in $Vldlr^{-/-}$ mice. These findings suggested that the photoreceptor c-Fos controls blood vessel growth into the normally avascular photoreceptor layer through the inflammatory signal–induced STAT3/VEGFA pathway.

INTRODUCTION

Pathological retinal angiogenesis is a leading cause of vision loss. The photoreceptor layer is a privileged zone devoid of vasculature to allow light to access photosensitive receptors. Photoreceptors lie between the highly organized but open lattice of vessels in the inner retina, which allows light through to photoreceptors, and the dense sinusoidal vascular plexus, the choriocapillaris, which lies beneath the retinal pigment epithelium (RPE). Both vascular beds are sources of neovascularization extending into the normally avascular photoreceptor and subretinal space between the RPE and the photoreceptor outer segments. The mechanisms by which photoreceptors maintain their avascular state are not well understood, but they are key to understanding neovascular eye diseases, including neovascular age-related macular degeneration (AMD) and macular telangiectasia (Klein et al., 2004). Abnormal blood vessels that extend into this privileged zone not only block light, but also disrupt retinal function to cause blindness (Luo et al., 2013).

Invasion of vessels into photoreceptors has been associated generally with increased inflammatory signals (Espinosa-Heidmann et al., 2003; Sakurai et al., 2003), but the timing and the localization of these signals are not well understood, particularly with respect to the initiation signals for neovascularization. Adaptive immunity and inflammation are highly controlled in the photoreceptor/subretinal space (Streilein et al., 2002; Masli and Vega, 2011), maintained by expression of immunosuppressive factors and characterized by lack of immune cells and, thereby, tolerance of foreign antigens (Streilein, 1995; Masli and Vega, 2011). Macrophages and dendritic cells are normally absent in the outer retina and are limited to the underlying choroidal vessels.

Eye diseases with pathological angiogenesis have a slow parainflammatory response (Medzhitov, 2008; Perez and Caspi, 2015), with changes in adaptive immunity and macrophage infiltration violating the normal ocular environment of immune privilege. In AMD, the blood–retinal barrier breaks down, and immune/inflammatory cells are recruited from the systemic circulation through the choroid or retinal vessels (Ambati et al., 2013) and accumulate in the subretinal space. Here, under stress conditions, they eliminate visual byprod-

ucts (Xu et al., 2008). In degenerative diseases, this breakdown in the immune privilege may be a compensatory response to maintain vision because impaired microglial migration into or out of the subretinal space promotes photoreceptor cell death (Combadière et al., 2007; Chen et al., 2011b). Loss of immune privilege may correlate with and increase neovascularization (Apte et al., 2006; Roychoudhury et al., 2010). We hypothesized that inflammatory signals from photoreceptors initiate the process to break down their avascular privilege, with secondary alterations in aspects of immune privilege. This mechanism might suggest novel molecular targets for anti-neovascular therapies directed at the initiation step.

The very low-density lipoprotein receptor–deficient ($Vldlr^{-/-}$) mouse is a model of pathological angiogenesis invading the avascular zone (Heckenlively et al., 2003; Li et al., 2007; Chen et al., 2009; Dorrell et al., 2009; Joyal et al., 2016). $Vldlr^{-/-}$ mice first develop retinal vascular lesions, invading photoreceptors from the retinal vessels, and then later develop choroidal neovascularization (also invading photoreceptors but from the choroidal vessels), associated with cone degeneration and then rod loss (Chen et al., 2009; Dorrell et al., 2009), retinal vascular leakage, and chronic inflammation, features similar to human neovascular AMD. Previous studies report that dysregulated photoreceptor energy metabolism (Joyal et al., 2016) and oxidative stress (Dorrell et al., 2009) contribute in part to increased levels of vascular endothelial growth factor A (VEGFA), which leads to neovascularization in $Vldlr^{-/-}$ retinas. Here, we used $Vldlr^{-/-}$ mice to explore the contribution of photoreceptor-specific inflammatory signals through c-Fos to control photoreceptor vascular privilege.

We postulated that c-Fos, a transcription factor that regulates many inflammatory signals, might control photoreceptor inflammation (Hoffman et al., 1993). c-fos encodes a nuclear DNA-binding phosphoprotein that forms heterodimeric complexes with members of the Jun family of proteins to constitute transcription factor complex activator protein 1 (AP-1; Curran and Franza, 1988; Hafezi et al., 1997). AP-1 regulates genes that affect the epidermal microenvironment, including cytokines such as IL-6, TNFα, and matrix proteins (Wagner and Eferl, 2005). c-fos is one of the immediate early genes (Hoffman et al., 1993) that are activated transiently and rapidly in response to a wide variety of cellular stimuli. c-Fos promotes inflammation and disease development in inflammatory diseases such as arthritis (Aikawa et al., 2008; Shiozawa and Tsumiyama, 2009), although it also acts as a negative regulator of inflammatory responses in myeloid and lymphoid cell lineages (Ray et al., 2006).

We found that photoreceptor c-Fos controlled vascular invasion into the photoreceptor layer in $Vldlr^{-/-}$ mice. Increased c-Fos in $Vldlr^{-/-}$ photoreceptors was associated with increased expression of its target genes including $Il6$ and Tnf, which led to activation of the STAT3/VEGFA pathway driven by both IL-6 and TNF/TNFα–induced protein 3 (TNFAIP3)/suppressor of cytokine signaling 3 (SOCS3) signals. Inhibition of c-Fos in photoreceptors using AAV (adeno-associated virus)–hRK (human rhodopsin kinase)–sh_c-fos blocked neovascularization in $Vldlr^{-/-}$ mice and rescued visual function. A chemical inhibitor of c-Fos also reduced neovascularization in $Vldlr^{-/-}$ mice. These findings suggested that photoreceptor c-Fos controls neovascularization through the neuronal STAT3/VEGFA pathway.

In summary, in the $Vldlr^{-/-}$ retina, in which vessels invade the avascular photoreceptor layer, c-Fos induced inflammatory signals in photoreceptors, leading to increased VEGF, which promoted neovascularization. Macrophage infiltration into the subretinal space occurred only in the late stage. c-Fos is hence a key factor that controls photoreceptor/subretinal space avascular and immune privilege and may be targeted to treat an initiating process in neovascular eye diseases.

RESULTS

In the photoreceptor layer of $Vldlr^{-/-}$ retina, inflammation is seen in association with neovascularization

There are three retinal vascular layers (superficial, intermediate, and deep) in the normal mouse retina (Fig. 1 A, left). In the $Vldlr^{-/-}$ retina, neovascularization extends from the retinal vasculature into the normally avascular photoreceptor layer by postnatal day 12 (P12) and reaches the RPE by P16 (Fig. 1 A). Newly formed vessels in adult $Vldlr^{-/-}$ retinas were leaky, as shown with fundus fluorescein angiography (FFA) at P30 (Fig. 1 B). These ectopic vessels reached the RPE and merged with the choroidal vessels to form retinal–choroidal anastomoses and choroidal neovascularization at ∼6–8 wk of age, violating the avascular privilege of the photoreceptor layer (Fig. 1 C). Later, in 3-mo-old adult (P90) $Vldlr^{-/-}$ retinas, IBA1-positive activated macrophages were seen infiltrating into the photoreceptor layer and subretinal space, indicating secondary loss of immune privilege (Fig. 1 D).

Elevated aqueous inflammatory cytokine levels are found in neovascular AMD patients (Roh et al., 2009). We examined inflammatory cytokine expression in WT and $Vldlr^{-/-}$ retinas at P12 as vessels began to invade photoreceptors. Total retinal mRNA of inflammatory cytokines $Il6$, Tnf, and $Il1\beta$ were markedly increased at P12 in $Vldlr^{-/-}$ versus WT retinas (Fig. 1 E). Yet, at this point, there were no detectable macrophages (a potential source of inflammatory cytokines) recruited into the photoreceptor layer and subretinal space (Fig. S1, A–C), as seen in P90 adult retinas (Fig. 1 D). At P12, there was no difference in the level of mRNA expression of macrophage markers including $Cd45$, $Cd11b$, $Cd68$, and $Cx3cr1$ between $Vldlr^{-/-}$ and WT retinas (Fig. S1 D). These data suggested that $Vldlr$ deficiency increased expression of inflammatory cytokines early (≤P12), before macrophage recruitment to the deep layer and the subretinal space, which was seen only at a later stage (3 mo). These results indicated that in $Vldlr^{-/-}$ retinas, neuronal cell inflammatory signals might initiate neovascularization, followed later by macrophage/immune cell recruitment (Fig. S1), which is consistent with our previous finding that there is no evidence for macrophage-induced onset of neovascularization (Joyal et al., 2016).
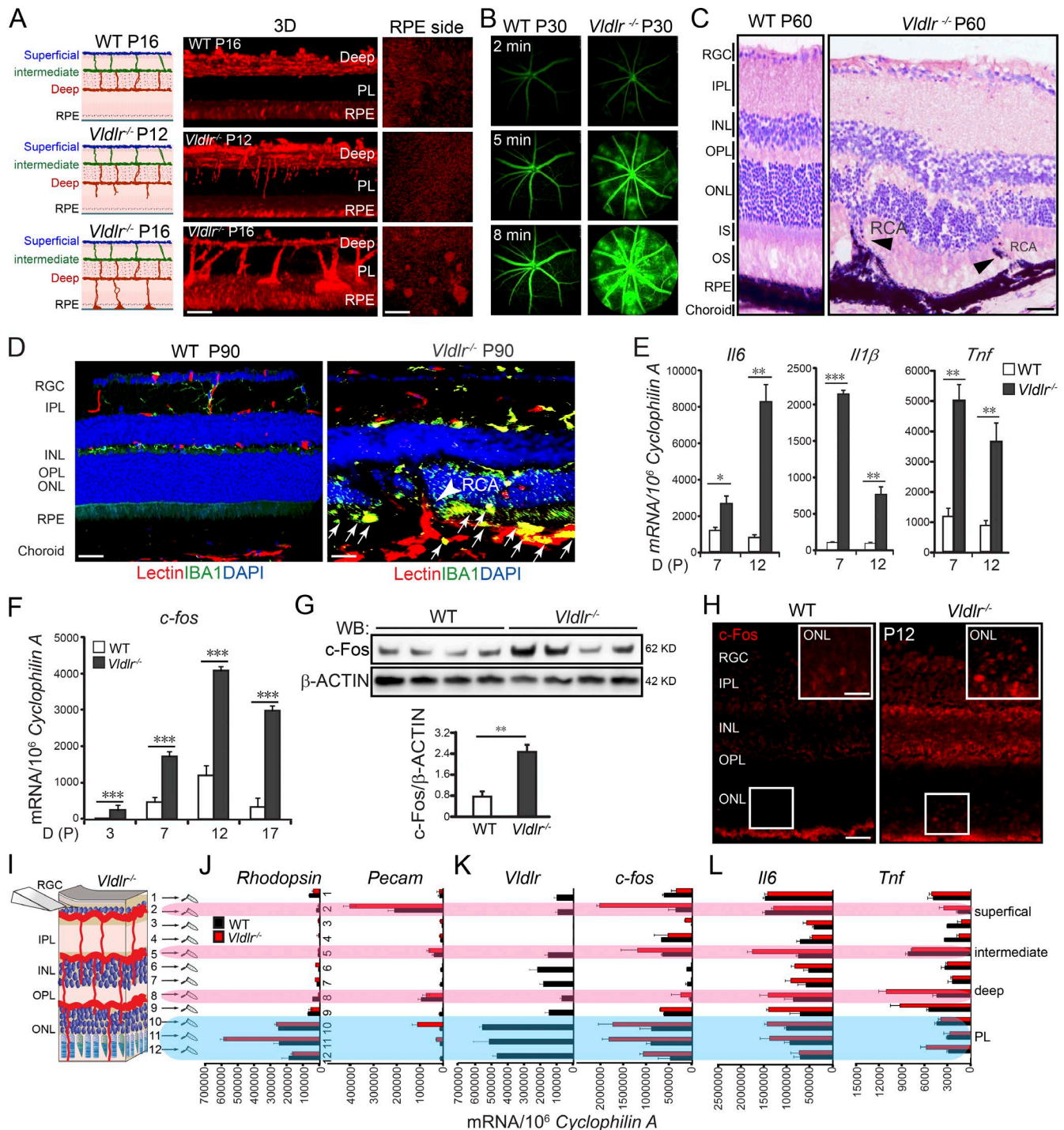
Figure 1. **c–Fos was induced in *Vldlr*−/− retinas.** (A) *Vldlr* deficiency led to neovascularization in the normally avascular photoreceptor layer shown by 3D reconstruction of representative confocal images. *n* = 6. (B) *Vldlr* deficiency led to retinal vascular leakage at 2, 5, and 8 min after intraperitoneal injection of fluorescent dye, as shown by FFA images from P30 WT and *Vldlr*−/− mice. *n* = 6. (C) H&E staining showed retinal layer disorganization and retinal–choroidal vascular anastomoses in P60 *Vldlr*−/− retinas. Black arrowheads indicate neovascularization. *n* = 6. (D) Macrophage marker IBA1 (green) costained with the endothelial cell marker isolectin (red) and nuclear marker DAPI (blue) in 3-mo *Vldlr*−/− retinas with retinal-choroidal vascular anastomoses (arrowhead); macrophages were seen in the subretinal space between the ONL and RPE (arrows). (E) Cytokine expression, including *Il6*, *Il1β*, and *Tnf*, was increased during development in *Vldlr*−/− retinas. *n* = 6. (F–L) *c-fos* mRNA and protein expression were markedly increased (F and G) in *Vldlr*−/− retinas during development (F), mainly in the P12 ONL (K) and colocalized with the expression of *Vldlr* in P12 WT (H–K) and its target genes including *Il6* and *Tnf* (L). *n* = 6. (H) IHC staining showed increased c-Fos expression in the ONL of P12 *Vldlr*−/− retinas. INL, inner nuclear layer; IPL, inner plexiform layer; IS, photoreceptor inner

c–Fos was highly induced in Vldlr⁻/⁻ retinas and si_c–fos reduced subretinal neovascularization

We examined inflammation as a possible mechanism underlying neovascularization (loss of immune/vascular privilege) in the photoreceptor layer in $Vldlr^{-/-}$ mice with microarray analyses. c-fos expression was markedly increased in P14 $Vldlr^{-/-}$ versus WT retinas (Table S1). We confirmed an increase in c-fos mRNA and protein levels in $Vldlr^{-/-}$ retinas before and during the development of pathological neovascularization (Fig. 1, F and G) with c-Fos immunohistochemistry staining (Fig. 1 H). c-Fos was highly induced in the outer nuclear layer (ONL; photoreceptors) in P12 $Vldlr^{-/-}$ retinas. To quantitatively localize c-fos, we developed a technique to tangentially section whole-mounted retinas and quantify mRNA in 12 individual cellular layers, from retinal ganglion cells to RPE (Fig. 1, I–L; and Fig. S2). The specificity and homogeneity of sectioned layers was confirmed by quantifying mRNA expression of $rhodopsin$ (photoreceptor marker) and platelet endothelial cell adhesion molecule ($Pecam$; vascular endothelial cell marker) in each layer (Fig. 1 J). Increased c-fos expression was mainly seen in the $rhodopsin$-expressing layers where $Vldlr$ was also highly expressed (Fig. 1 K). c-fos expression was also increased in layer 2, which mainly contained superficial vessels and retinal ganglion cells, suggesting that c-fos may also play a role in cells other than photoreceptors, which needs further study. Target inflammatory genes of c-fos, $Il6$, and Tnf were identified mainly in the same layer as $Vldlr$ and c-fos, suggesting that VLDLR/c-Fos might mediate the disruption of angiostatic privilege in the retinal photoreceptor layer by controlling local photoreceptor inflammatory signals (Fig. 1 L). In addition, the expressions of $Il6$ and especially Tnf were also increased in layers 8 and 9, which contain the deep layer of retinal vessels. This increase might arise from proliferating endothelial cells, as the deep layer of vessels form at that time.

To suppress increased c-fos expression, we used pooled si_c-fos comprising three siRNA sequences. The knockdown efficiency was confirmed to be ∼65% in photoreceptor 661W cells (Fig. S3 A). Subretinal injection of the si_c-fos pool suppressed both mRNA and protein expression of c-fos in the P12 $Vldlr^{-/-}$ photoreceptor layer by ∼40–50% (Fig. S3, B and C), associated with a reduction in neovascularization in the photoreceptor layer (Fig. S3 D). Three-dimensional (3D) reconstruction of representative confocal images of retinal whole mounts stained with the endothelial cell marker isolectin IB₄ showed 45% fewer vascular lesions reaching the RPE, which lies beneath the photoreceptors (Fig. S3, D and E). The mean lesion size was also reduced (Fig. S3 F). Thus, knockdown of c-fos inhibited neovascularization in $Vldlr^{-/-}$ retinas.

AAV expressing sh_c–fos in the photoreceptor layer inhibited neovascularization and preserved retinal function

Because of nonspecific targeting and the transient effect of siRNA, si_c-fos could neither specifically nor efficiently target photoreceptor cells (Fig. S3). Therefore, we generated a photoreceptor-specific AAV2 carrying shRNA of c-fos with the hRK promoter (Fig. 2 A; Khani et al., 2007). Three shRNA sequences were cloned, and the knockdown efficiency was validated using photoreceptor 661W cells (Fig. S3 G). We injected AAV2-hRK–sh_c-fos subretinally at P1 and evaluated retinas at P16 (Fig. 2 B). The infection was confirmed with anti-GFP antibody staining in the photoreceptor layer and subretinal space (Fig. 2 C), showing that 75–80% of the retina was successfully transfected with AAV (Fig. 2 C). Consequently, both mRNA and protein expression of c-fos were reduced by ∼60% (Fig. 2, D and E), and neovascularization was reduced by >70% at P16 (Fig. 2, F and G), as measurements included total retinal areas, which may not be completely affected by AAV2-hRK–sh_c-fos (∼25% not transfected) as shown (Fig. 2, C and F, white arrowhead). The mean lesion size was reduced by 83% (Fig. 2, F–H). AAV2-hRK–sh_c-fos treatment also prevented vessel leakage (Fig. 2 I). These results suggest that c-Fos and VLDLR functioned synergistically in maintaining photoreceptor avascular privilege. Moreover, AAV2-hRK–sh_c-fos significantly rescued visual dysfunction in $Vldlr^{-/-}$ mice. Untreated $Vldlr^{-/-}$ mice were characterized by lower electroretinographic photoreceptor sensitivity (a–waves) than age-matched WT mice. AAV2-hRK–sh_c-fos injection improved photoreceptor sensitivity at 3 mo after injection compared with AAV2-hRK–$sh\_control$–injected $Vldlr^{-/-}$ mice (Fig. 2 J), indicating protection of photoreceptor function.

c–Fos promoted retinal angiogenesis via the neuronal STAT3/VEGF pathway

IL-1β and TNF increase the expression of VEGF (Margetts et al., 2002); c-Fos transcriptionally regulates VEGF production in peritoneal inflammation via IL-1β and TNF (Catar et al., 2013). We found that increased levels of $Il6$ (Fig. 1 E), a transcriptional target of c-Fos, activated STAT3 and increased expression of $Vegfa$ isoforms $Vegf120$ and $Vegf164$ (Fig. 3 A), which likely contributed to the neovascularization in $Vldlr^{-/-}$ retinas. $Vegfa$ expression was markedly increased in $Vldlr^{-/-}$ mice at P12 and P17, as well as in the P12 photoreceptor layer of $Vldlr^{-/-}$ retinas (Fig. 3, B and C). VEGFA was reduced by $AAV2$-hRK–sh_c-fos in $Vldlr^{-/-}$ retinas (Fig. 3 D), which was associated with activated (phosphorylated) STAT3 and increased IL-6. We also knocked down VEGFA expression in photoreceptors using AAV2-hRK-sh_Vegfa, which strongly suppressed neovascu-
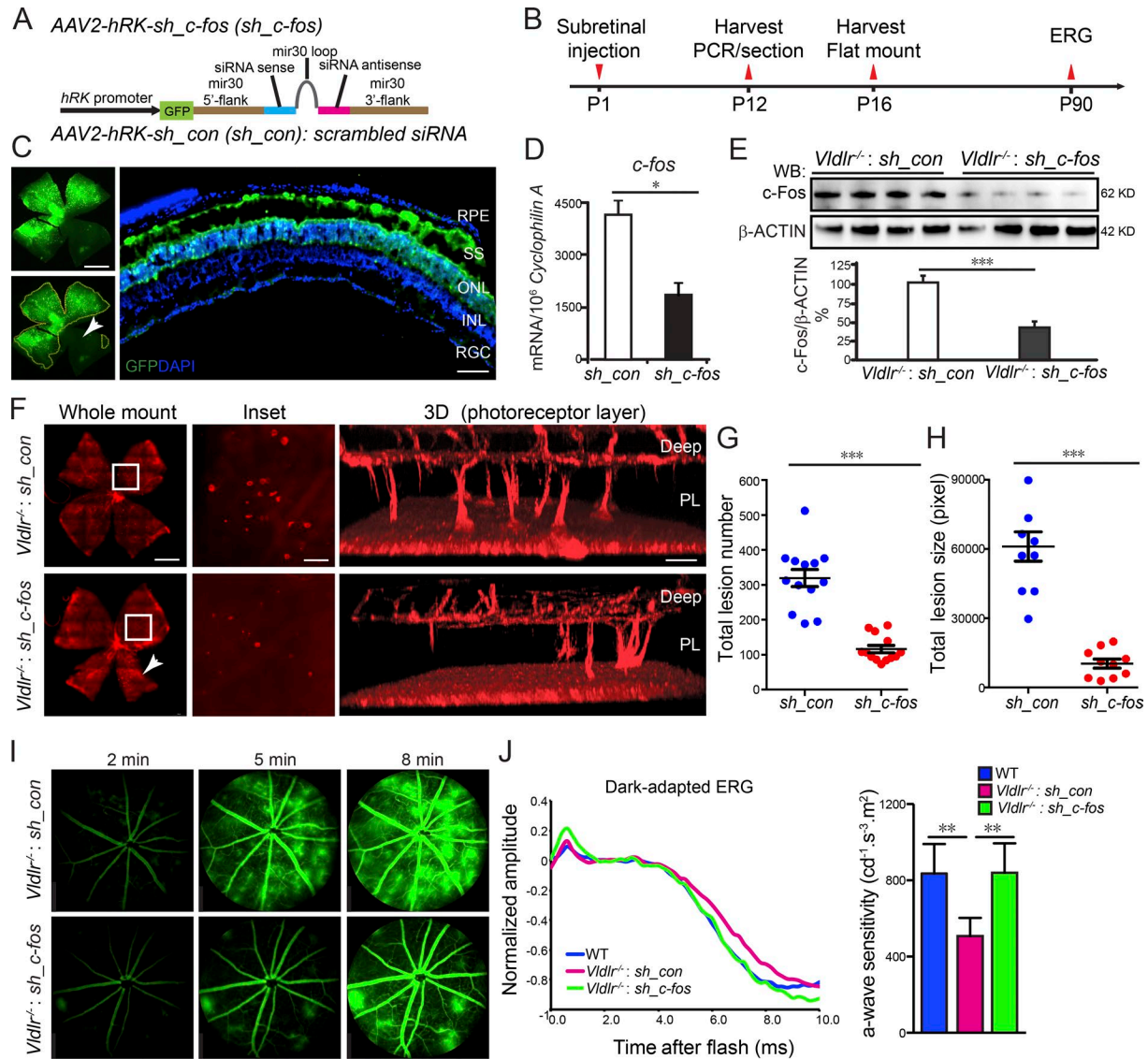
Figure 2. **Attenuation of c–Fos in the photoreceptor layer extending to the subretinal space reduced neovascularization.** (A) Schematic diagram illustrating AAV2 carrying *sh_c-fos* within a mir30 cassette under the control of an *hRK* promoter (*hRK-sh_c-fos*). sh_con, sh_control. (B) Time line for AAV subretinal injection and retina collection. (C) The infection of AAV2 in the subretinal space (SS) and photoreceptor layer was confirmed by AAV2-*hRK-eGFP*. *n* = 6. INL, inner nuclear layer; RGC, retinal ganglion cell. The white arrowhead indicates the retinal areas were not affected by AAV2-*hRK-eGFP* because of the limitation of subretinal injection. (D and E) The knockdown efficiency of *AAV2-hRK-sh_c-fos* via subretinal injection into *Vldlr⁻/⁻* retinas was confirmed by comparison with AAV2-*hRK-sh_control*–injected retinas at both mRNA (D) and protein (E) levels. (D) *, P < 0.05. *n* = 6. (E) ***, P < 0.001. *n* = 4. WB, Western blot. (F) Knocking down *c-fos* in the photoreceptor layer (PL) extending to the subretinal space using *AAV2-hRK-sh_c-fos*–inhibited neovascularization shown by whole-mounted images of AAV2-*hRK-sh_control*– or *AAV2-hRK-sh_c-fos*–treated *Vldlr⁻/⁻* retinas stained with isolectin IB4 to label endothelial cells and representative 3D reconstruction images for neovascularization in photoreceptor layers, including the retinal areas, which may not be completely affected by AAV2-*hRK-sh_c-fos* (about 25% not transfected) as shown in C (white arrowhead in C and F). (G and H) Both total lesion number and total lesion size (pixels) were reduced in *AAV-hRK-sh_c-fos*–treated compared with AAV2-*hRK-sh_control*–treated retinas. ***, P < 0.001. *n* = 8–13. (I) *AAV2-hRK-sh_c-fos* injected in the subretinal space at P1 rescued *Vldlr* deficiency–induced retinal vascular leakage shown by FFA images at P60 in *Vldlr⁻/⁻*–treated mice. *n* = 6–8. (J) Representative dark-adapted (scotopic) ERG graph (left) and quantification of photoreceptor a-wave sensitivity (right) showed that photoreceptor function was attenuated in 3-mo-old *Vldlr⁻/⁻* retinas and was particularly rescued by *AAV-hRK-sh_c-fos* (one-time treatment on P1) in 3-mo-old *Vldlr⁻/⁻* retinas. *, P < 0.05; **, P < 0.01; ***, P < 0.001. Bars: (C and F, whole-mount images) 1,000 μm; (C, cross section) 50 μm; (F, inset) 250 μm; (F, 3D) 100 μm. All data are representative of at least three independent experiments. Results are presented as mean ± SEM.
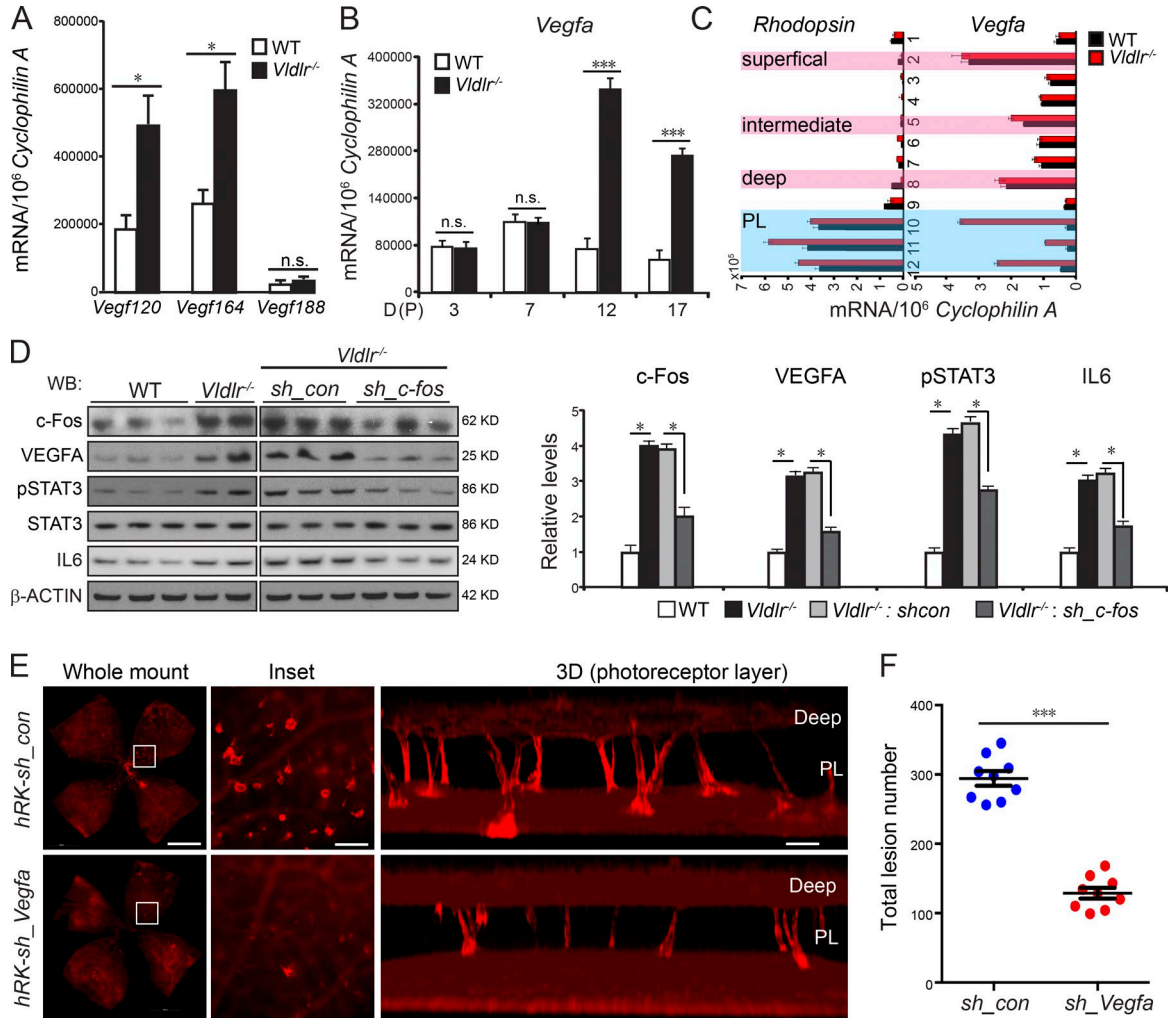
Figure 3. **c–Fos promoted retinal angiogenesis via VEGFA signaling modulated by neuronal IL–6/STAT3.** (A) *Vegf120* and *Vegf164* but not *Vegf188* expression was increased in P12 *Vldlr*$^{-/-}$ retinas. $n = 6$. (B and C) *Vegfa* expression was markedly increased in *Vldlr*$^{-/-}$ whole retinas at P12 and P17 (B) as well as in the photoreceptor layer (PL) of P12 *Vldlr*$^{-/-}$ retinas (C). $n = 6$. (D) The protein levels of c-Fos, pSTAT3, total STAT3, IL-6, and VEGFA in P12 WT, *Vldlr*$^{-/-}$, and *Vldlr*$^{-/-}$ treated with *AAV2-hRK-sh_c-fos* or *AAV2-hRK-sh_control* (sh_con). $n = 4$–6. WB, Western blot. (E and F) Representative P16 whole mount images stained with isolectin IB4 and quantification showed that knocking down VEGFA in *Vldlr*$^{-/-}$ retinas using AAV2-*hRK-sh_Vegfa* reduced total lesion number by 55% compared with *AAV2-hRK-sh_control*–treated *Vldlr*$^{-/-}$ retinas. (E) Bars: (whole-mount images) 1,000 µm; (inset) 250 µm; (3D) 100 µm. PL, photoreceptor layer. All data are representative of at least three independent experiments. *, $P < 0.05$; ***, $P < 0.001$. Results are presented as mean ± SEM.

larization in *Vldlr*$^{-/-}$ retinas (Fig. 3, E and F), suggesting that VEGFA from photoreceptors directly caused neovascularization, consistent with previous studies (Usui et al., 2015; Joyal et al., 2016). Therefore, it is likely that c-Fos promoted neovascularization in the photoreceptor layer via VEGFA signaling, which may be driven by IL-6/STAT3.

TNFAIP3, a gene important in cytokine-mediated immune and inflammatory responses, is induced by TNF, another c-Fos target gene. We found that TNFAIP3 was induced at both mRNA and protein levels in *Vldlr*$^{-/-}$ retinas (Fig. 4, A and B), concomitant with increased *Tnf*. Interestingly, TNFAIP3 is reported to suppress SOCS3 expression to enhance STAT3 proliferative signals (da Silva et al., 2013).

We found that *Vldlr*$^{-/-}$ retinas have less SOCS3 expression than WT (Sun et al., 2015b). These findings suggested that STAT3 could also be activated by increased *Tnf*/*Tnfaip3* signals that further led to reduced *Socs3* level in *Vldlr*$^{-/-}$ retinas. Here, we showed that overexpression of *Socs3* mainly in the photoreceptor layer reduced neovascularization in *Vldlr*$^{-/-}$ retinas (Fig. 4, C–F). These results suggested that SOCS3 is critical to neovascularization and that reduction of SOCS3 expression in *Vldlr*$^{-/-}$ versus WT retinas may be secondary to up-regulation of *Tnf*/*Tnfaip3* induced by *c-fos*. SOCS3 inhibits activation of STAT3 by binding to the kinase JAK and the IL-6 receptor (Wei et al., 2014), which induces the expression of VEGF (Wei et al., 2003). Consistently, we found
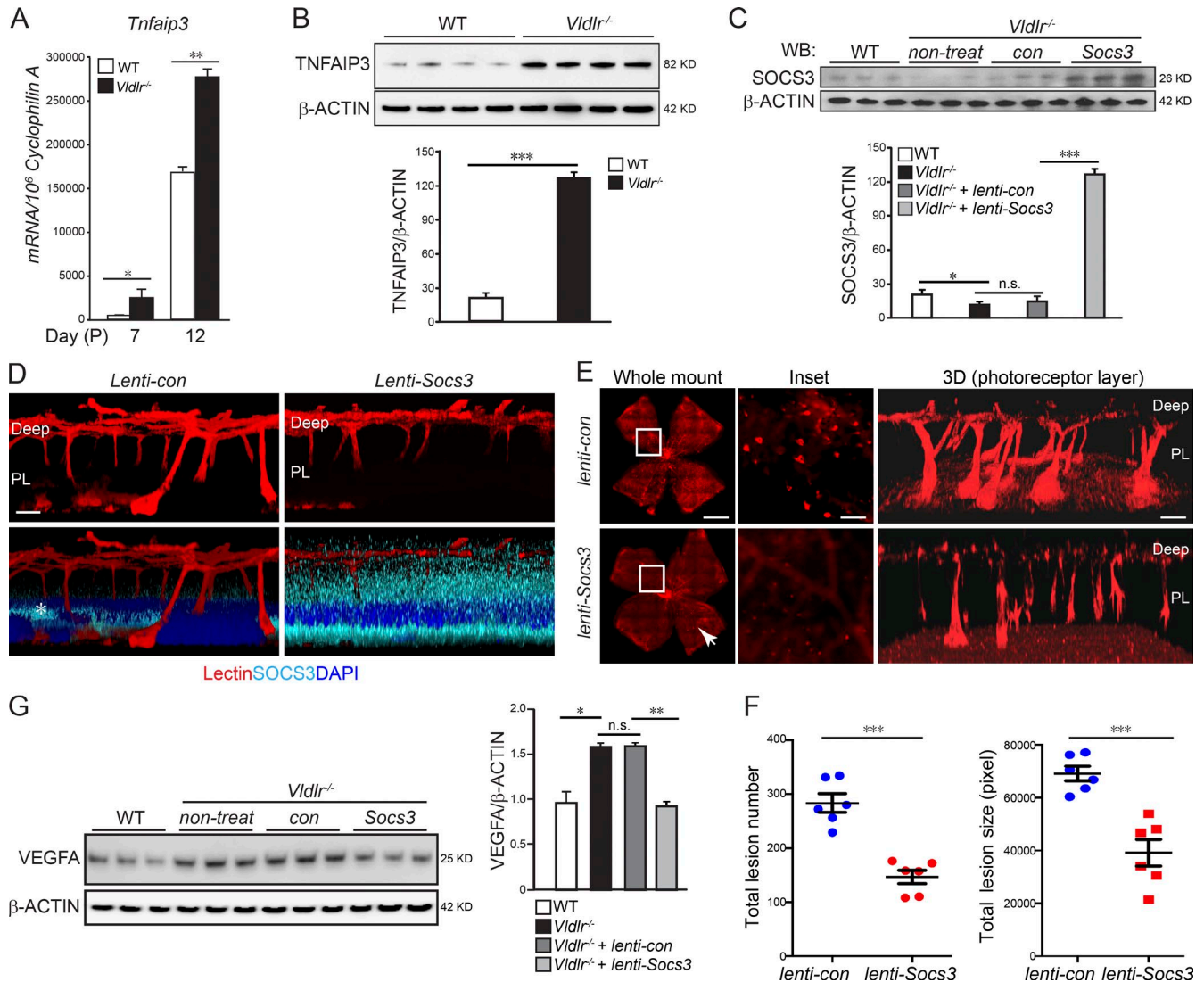
Figure 4. **c–Fos promoted retinal angiogenesis via TNF/TNFAIP3/SOCS3.** (A and B) *Tnfaip3* mRNA (A; *n* = 6) and protein levels (B; *n* = 4) were increased in the developing *Vldlr*^{−/−} retinas compared with WT controls. (C) *Lenti-Socs3* was injected subretinally into *Vldlr*^{−/−} eyes, and SOCS3 protein levels were confirmed by Western blotting (WB). *n* = 3. con, control; non-treat, nontreated. (D) The infection of *lenti-Socs3* in the photoreceptor layer (PL) was confirmed by anti-SOCS3 antibody staining (cyan). 3D reconstructed representative images show that SOCS3 was mainly expressed in the photoreceptor layer after subretinal injection. *n* = 4. The asterisk in the lenti-control image indicates nonspecific staining. (E and F) Overexpression of Socs3 using *lenti-Socs3* inhibited neovascularization, including the retinal areas, which may not be completely affected by *lenti-Socs3* (~25% not transfected; white arrowhead). (E) The representative whole-mount images of *lenti-control*– or *lenti-Socs3*–treated *Vldlr*^{−/−} retinas stained with isolectin IB4 to label endothelial cells. 3D reconstruction images show neovascularization in the photoreceptor layer. *n* = 6. (F) Quantification shows a decrease in both total lesion number and total lesion size in *lenti-Socs3*–treated *Vldlr*^{−/−} retinas compared with lenti-control–treated *Vldlr*^{−/−} retinas. *n* = 6. (G) Increased protein level of VEGFA in *Vldlr*^{−/−} retinas was suppressed by *lenti-Socs3* treatment. *n* = 3. Bars: (E, whole-mount images) 1,000 µm; (E, inset) 250 µm; (D and E, 3D) 100 µm. All data are representative of at least three independent experiments. *, P < 0.05; **, P < 0.01; ***, P < 0.001. Results are presented as mean ± SEM.

that, in *Vldlr*^{−/−} retinas, overexpression of *Socs3* suppressed the increased VEGFA level by ~45% (Fig. 4 G).

To confirm that c-Fos activates the STAT3/VEGFA pathway via IL-6 and TNF/TNFAIP3/SOCS3 signals in retinal photoreceptors, we examined *Vldlr*-deficient 661W photoreceptor cells (treated with AAV2-hRK-shRNA targeting *Vldlr*). Knocking down *Vldlr* increased mRNA expression of *c-fos*, *Il6*, *Tnf*, *Tnfaip3*, and *Vegfa*, also decreasing *Socs3*. In *Vldlr*^{−/−} retinas, *AAV2-hRK–sh_c-fos* treatment restored *Il6*, *Tnf*, *Tnfaip3*, *Vegfa*, and *Socs3* expression to normal levels (Fig. 5, A–G). Thus, c-Fos in photoreceptors promoted retinal neovascularization via the neuronal STAT3/VEGF pathway induced by IL-6 and TNF/TNFAIP3/SOCS3 signals (Fig. 5 H).
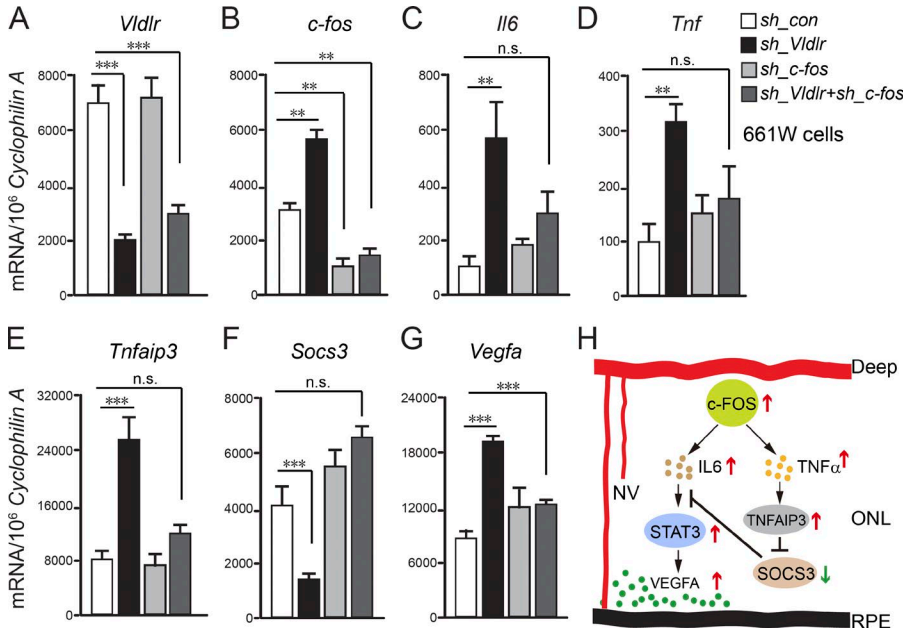
Figure 5. **c-Fos regulated Vegfa via TNF/ TNFAIP3/SOCS3 in photoreceptor cells.** (A–G) The mRNA levels of *Vldlr*, *c-fos*, *Il6*, *Tnf*, *Tnfaip3*, *Socs3*, and *Vegfa* in 661W photoreceptor cells treated with *AAV2-hRK-sh_Vldlr* and/or *AAV2-hRK–sh_c-fos* or *AAV2-hRK-sh_Control* (sh_con). **, $P < 0.01$; ***, $P < 0.001$. $n = 6$. (H) A schematic diagram illustrates pathological neovascularization (NV) in the normal avascular photoreceptor layer controlled by transcriptional factor c-FOS through both IL-6/STAT3/VEGFA and TNF/TNFAIP3/SOCS3/ STAT3/VEGFA pathways. All data are representative of at least three independent experiments. Results are presented as mean ± SEM.

As c-Fos and c-Jun proteins form the AP-1 complex (Chinenov and Kerppola, 2001), we also assessed the expression of *c-jun*, the levels of which were comparable between WT and $Vldlr^{-/-}$ retinas (Fig. S4). In addition, mRNA expression of urokinase-type plasminogen activator (*uPA*) was markedly increased in $Vldlr^{-/-}$ retinas (Fig. S4 B), suggesting that it might be a potential factor underlying high levels of transcription factor *c-fos* expression.

We previously found that energy deficiency in photoreceptors, which is exacerbated in the dark because of increased energy demand of the dark current, also causes an increase in photoreceptor VEGF and increased neovascularization in $Vldlr^{-/-}$ mice (Joyal et al., 2016). *c-fos* mRNA expression increased ∼10-fold at P8 and 20-fold at P12 in dark-reared (vs. 12 h dark/light control) $Vldlr^{-/-}$ mice (Fig. S4 C), suggesting that *c-fos* expression may also be mediated by increased photoreceptor energy demands of dark rearing in $Vldlr^{-/-}$ mice.

Pharmacologic inhibition of c-Fos suppressed retinal neovascularization

SR11302 is a retinoid that specifically inhibits AP-1 activity without activating the transcription of retinoic acid response element (Fig. 6 A; Fanjul et al., 1994). AP-1 consists of a family of c-Jun/c-Fos dimers that include different Jun proteins (c-Jun, JunB, and JunD) and Fos proteins (c-Fos, FosB, FosL1, FosL2, and FosB2; Angel and Karin, 1991). The efficiency of SR11302 on AP-1 inhibition in SR11302-treated retinas was confirmed with the reduction of c-Fos target gene expression (*Il6*, *Il1β*, and *Tnf*), without a change in *c-fos* expression itself (Fig. 6 B). SR11302 treatment reduced the total vascular lesion number and lesion size in $Vldlr^{-/-}$ mice in a dose-dependent manner. High-dose SR11302 from P5 to P15 in $Vldlr^{-/-}$ mice reduced the total vascular lesion number

by 48% and decreased the lesion size by 40% (Fig. 6, C–E), without detectable signs of toxicity in mice, including no change in body weight (Fig. S5).

DISCUSSION

Here, we identify photoreceptors as the source of inflammatory signals that regulate the disruption of avascular privilege and later the disruption of immune privilege in photoreceptors in $Vldlr^{-/-}$ mice. We show that increased *c-fos* and inflammatory signals in the $Vldlr^{-/-}$ photoreceptor layer were associated with neovascularization invading a normally avascular-privileged zone, followed later by macrophage migration into the photoreceptor/subretinal space. Reducing *c-fos* expression suppressed local photoreceptor-produced proinflammatory cytokines and prevented neovascularization. Thus, photoreceptor inflammatory signals initiated neovessel growth into the avascular zone. It is plausible that *c-fos* could promote and *c-fos* inhibitors could suppress neovascularization in many eye diseases. The theoretical advantage in suppressing c-Fos (or AP-1) to suppress downstream targets (which include VEGF) rather than suppressing VEGF directly is that many AMD patients do not respond to anti-VEGF treatment and that inflammation is also a target in pathological retinal angiogenesis in neovascular eye diseases.

Although retinal inflammation is clearly involved in AMD, the relevant cells and pathways have not been fully defined. In $Vldlr^{-/-}$ mice, increased leukostasis and elevated levels of proinflammatory factors, such as intercellular adhesion molecule 1, TNF, endothelial nitric oxide synthase, and cyclooxygenase 2, indicate the presence of inflammation (Chen et al., 2009). We showed a direct role for photoreceptor c-Fos (or AP-1) in promoting pathological vasculature in the photoreceptor avascular-privileged zone through photorecep-
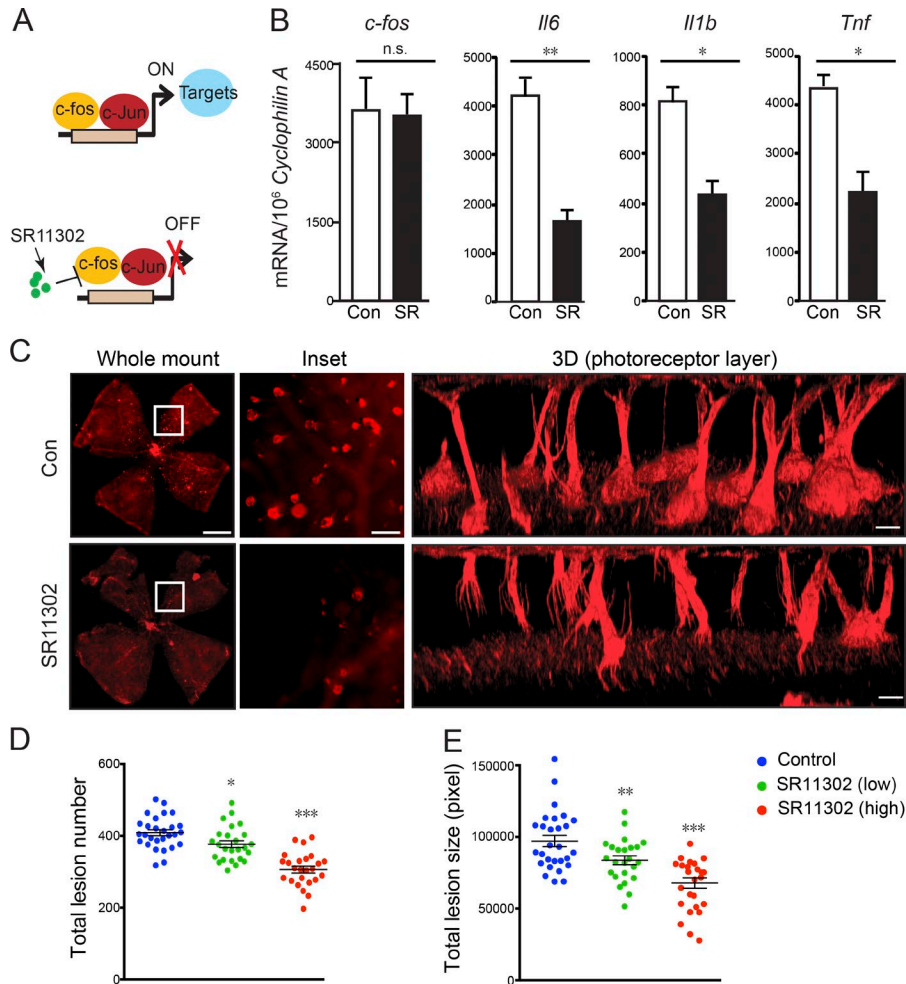
Figure 6. **c-Fos inhibitor SR11302 prevented retinal neovascularization.** (A) Schematic diagram illustrating how c-Fos inhibitor SR11302 may block c-Fos binding to its target promoters to inhibit target gene expression. (B) The mRNA levels of *c-fos* and its target genes (*Il6*, *Il1β*, and *Tnf*) in SR11302 (SR)-treated and control (con) *Vldlr*$^{-/-}$ retinas confirmed the efficiency of the c-Fos inhibitor. *n* = 6. (C) SR11302 inhibited neovascularization. Representative whole-mount images of control or SR11302-treated *Vldlr*$^{-/-}$ retinas stained with isolectin IB4 to label endothelial cells. Enlarged images show reduced total lesion number and lesion size in the SR11302-treated retinas. 3D reconstruction images show neovascularization in the photoreceptor cell layer. Bars: (whole-mount images) 1000 µm; (inset) 250 µm; (3D) 100 µm. (D and E) Quantification shows reduced total lesion number and lesion size (pixels) in SR11302-treated retinas compared with controls in a dose-dependent manner. *n* = 22–29. All data are representative of at least three independent experiments. *, P < 0.05; **, P < 0.01; ***, P < 0.001. Results are presented as mean ± SEM.

tor-derived inflammatory mediators. AP-1 positively regulates the expression of inflammatory mediators such as IL-6 and TNF in a variety of cells (Lee et al., 2004). The AP-1 complex is prototypically a c-Fos and c-Jun protein dimer (Chinenov and Kerppola, 2001). In contrast to c-Jun proteins, c-Fos subunits cannot form homodimers but require combination with other binding proteins. In *Vldlr*$^{-/-}$ retinas, we found increased expression of *c-fos* but not of *c-jun*, which is likely to enlarge the pool of c-Fos available for heterodimerization and increase the fraction of AP-1 complexes composed of c-Fos and c-Jun (Catar et al., 2013). This may directly affect proinflammatory cytokines gene expression, as complexes of c-Fos and c-Jun bind more effectively to target DNA sequences than c-Jun homodimers (Halazonetis et al., 1988). However, inflammatory cytokines including IL-6, TNF, and IL-1β can induce a rapid and transient expression of mRNA encoding c-Fos (McKay et al., 2001). In *Vldlr*$^{-/-}$ retinas, the positive feedback loop of *c-fos* and cytokine-mediated inflammatory signals induced neovascularization. To explore the importance of this feedback loop in neovascularization, we broke down the positive feedback loop through subretinal injection of lentivirus expressing SOCS3, which inhibited STAT3 activation in *Vldlr*$^{-/-}$ retinas. Overexpression of SOCS3 led to reduced cytokine production and a 50% reduction of neovascularization in *Vldlr*$^{-/-}$ retinas. These findings suggest that the feedback loop of *c-fos*/inflammatory cytokines plays a critical role in *Vldlr* deficiency–induced neovascularization. This is consistent with our previous study (Sun et al., 2015b) showing that induction of retinal *Socs3* expression with a synthetic inverse agonist of retinoic acid receptor–related orphan receptor α (RORα) inhibited subretinal neovascular lesions in *Vldlr*$^{-/-}$ retinas.

The complex of uPA and plasminogen activator inhibitor 1 is one of the VLDLR ligands. It can promote cell proliferation and migration by activating the extracellular signal–regulated kinase pathway (Webb et al., 2001). The plasminogen and plasminogen activator system consists of serine proteases that regulate migratory and tissue-remodeling events, such as those observed in neovascular AMD (Pepper, 2001). uPA mRNA is expressed in both choroidal neovascularization membranes extracted from patients with neovascular AMD and in experimentally induced choroidal neovascularization in mice (Rakic et al., 2003; Balasubramanian et al., 2014). Increases in uPA are reported in patients with neovascular AMD

(Sung et al., 2012). However, the role of uPA in neovascular AMD is largely unknown. Binding of uPA to its receptor uPAR induces the rapid but transient expression of *c-fos* in human ovarian cancer cells (Dumler et al., 1994). This signal generates protein tyrosine kinase activity feeding into a signal transduction pathway that activates nuclear transcription factors (Dumler et al., 1994). Our data suggest that increases in free uPA caused by *Vldlr* deficiency (Fig. S4 B) might potentially induce expression of high levels of *c-fos*.

Our previous study (Joyal et al., 2016) found that dark-reared *Vldlr*$^{-/-}$ mice develop 1.5-fold more vascular lesions than 12-h light and dark cycle–raised mice, suggesting that energy metabolism influences neovascular disease, as dark rearing increases the energy demand of the dark current in photoreceptors (Ames et al., 1992). In this study, we found that *c-fos* mRNA expression increased >10-fold in dark-reared (vs. 12 h dark/light control) *Vldlr*$^{-/-}$ mice (Fig. S4 C), which suggests that *c-fos* expression is also mediated by increased photoreceptor energy demands of dark rearing in *Vldlr*$^{-/-}$ mice. There is a strong correlation between mRNA levels of *c-fos* in the ONL (photoreceptors) and the genes coding for the phototransduction proteins related to diurnal changes (Nir and Agarwal, 1993). In rat retinas, *c-fos* mRNA is transiently expressed in the inner nuclear layer and ganglion cell layer after the onset of the light period and expressed continuously in the ONL throughout the dark period under a light/dark (12/12 h) cycle (Yoshida et al., 1993). This relationship suggests that *c-fos* may also play a role in the transcriptional regulation of the genes encoding these light/dark cycle proteins (Ohki et al., 1996).

Our previous study (Joyal et al., 2016) shows that activation of the free fatty acid receptor 1 (*Ffar1*) impairs glucose entry into photoreceptors resulting in a dual (lipid and glucose) fuel shortage in *Vldlr*$^{-/-}$ mice that have impaired lipid uptake. This energy shortage results in a reduction in the levels of the Krebs cycle intermediate α-ketoglutarate, which promotes stabilization of hypoxia-induced factor 1α and secretion of VEGF by starved *Vldlr*$^{-/-}$ photoreceptors, leading to neovascularization. However, the double knockout *Vldlr*$^{-/-}$/*Ffar1*$^{-/-}$ did not completely suppress the lesions, indicating that there are other pathways involved in this process. This study showed that *c-fos*–driven inflammation signals might also be induced during this energy-deprived process to control photoreceptor VEGF secretion.

Anti-VEGF drugs are widely used clinically to control the proliferation of pathological blood vessels driven by high levels of VEGF. However, basal levels of VEGF are needed for neuron and normal vessel survival. Under such circumstances, blocking only excess but not all VEGF will be very helpful. Targeting c-Fos or SOCS3 may prevent photoreceptor cells from releasing excessive VEGF without affecting its basal level.

c-fos$^{-/-}$ mice were reported to have reduced brain size because of apoptosis at the ventricular zone (Velazquez et al., 2015), and retina from *c-fos*$^{-/-}$ mice have 23% fewer rod photoreceptor cells with 25% lower rhodopsin content (Kueng-Hitz et al., 2000), suggesting *c-fos* is required for protection against cell apoptosis and that complete suppression of *c-fos* may be detrimental. We suppressed increased c-Fos using *si_c-fos*, *AAV2-hRK–sh_c-fos*, and SR11302 to control neovascularization in *Vldlr*$^{-/-}$ photoreceptors. Based on Fig. 3 D, the protein level of c-Fos after *AAV2-hRK–sh_c-fos* treatment for 3 mo was little higher than but comparable with that in WT, suggesting that normalization of the large increase in c-Fos seen with pathological neovascularization rather than complete suppression would be of benefit.

In summary, this study demonstrated that photoreceptor inflammatory signals initiate the vision-threatening invasion of blood vessels into an avascular-privileged zone in the retina. Retinal photoreceptor transcription factor c-Fos controls local inflammatory signaling to mediate neovascularization. Targeting the transcription factor c-Fos might be a novel way to prevent vision loss secondary to pathological retinal angiogenesis and may have broad therapeutic value for other vascular disorders involving photoreceptor microenvironmental inflammation.

MATERIALS AND METHODS
Animals
All animal studies were performed according to protocols approved by the Institutional Animal Care and Use Committee at the Boston Children's Hospital. Mice were housed under specific pathogen–free conditions. *Vldlr*$^{+/-}$ (heterozygous) mice from The Jackson Laboratory (stock no. 002529) were crossed to generate homozygous and WT littermates. SR11302 (cat. 2476; Tocris Bioscience) was dissolved in corn oil. *Vldlr*$^{-/-}$ pups were orally gavaged with SR11302 or vehicle control (corn oil) at two doses (low dose 0.5 mg/kg body weight and high dose 1 mg/kg body weight) daily from P5 to P15. P16 retinas were collected for PCR and neovascularization analysis.

Neovascularization analysis
Vldlr$^{-/-}$ and WT retina whole mounts were stained with isolectin IB4 and imaged with a microscope (AxioObserver. Z1; ZEISS) with a monochrome digital camera (AxioCam MRm; ZEISS) focusing on the terminal end of lesions on the RPE layer (usually at P16), and individual images were merged to create one retinal image using the automated merge function (mosaiX; ZEISS) in the software (AxioVision 4.6.3.0; ZEISS). ImageJ (National Institutes of Health) was used for quantification of subretinal neovascularization lesion number and areas in *Vldlr*$^{-/-}$ retinas with designed plugins adapted from the method used to measure retinal neovascularization (SWIFT_ MACTEL) in the oxygen-induced retinopathy model (Stahl et al., 2009; Joyal et al., 2016). In brief, SWIFT_MACTEL isolates the red channel from a lectin-stained retinal whole mount, divides the image into four quadrants, and removes background fluorescence to allow for the neovascularization structures to stand out clearly against the background fluorescence of normal vessels. Using a slide

bar to either increase or decrease a particular quadrant's fluorescence threshold, the SWIFT_MACTEL user designates a threshold that marks neovascularization structures but not normal vessels in each quadrant. After setting the appropriate threshold, artifacts like cellular debris or hyperfluorescent retinal edges can be manually removed and excluded from quantification. Then, SWIFT_MACTEL analyzes all pixels in the image that lie above the chosen intensity threshold and that are part of an object that has a minimum size of 100 pixels. By setting this cut off in object size, small artifacts like vessel branch points are automatically removed. After measuring all four quadrants, SWIFT_MACTEL creates a composite from all four neovascularization quadrants and calculates the total neovascularization pixel number. The *n* number is the number of eyes quantified. Lesion numbers and areas were quantified with researchers masked to the identity of samples.

Confocal imaging and 3D reconstruction
At P16, mice were anesthetized, and the eyes were enucleated and fixed in 4% paraformaldehyde followed by dissection and staining of the retinas with fluoresceinated isolectin IB4 (Invitrogen) to visualize subretinal neovascularization in whole-mounted retinas. 3D reconstructed images were taken with confocal microscopy (TCS SP2 AOBS; Leica Biosystems), and z stacks were 3D reconstructed using Volocity software (PerkinElmer).

FFA
Mice were anesthetized and injected intraperitoneally with fluorescein AK-FLUOR (Akorn) at 5 µg/g body weight. Fluorescent fundus images with dilated pupils were taken with a retinal-imaging microscope (Micron IV; Phoenix Research Laboratories) at 5 and 8 min after fluorescein injection.

Expression array
Illumina mouse gene microarray analysis of P14 WT and $Vldlr^{-/-}$ retinas was performed in biological triplicate (Mouse-WG6 expression BeadChip; Illumina). The chip contains 45,000 probe sets representing 34,000 genes. Microarray studies, from cDNA synthesis to raw data normalization, were performed by the Molecular Genetics Core Facility at Boston Children's Hospital. In brief, total RNA (1 µg each) was reverse transcribed, followed by a single in vitro transcription amplification to incorporate biotin–labeled nucleotide, and subsequent hybridization and staining with strepatavidin-Cy3 was performed according to the manufacturer's instructions. The chip was scanned with a BeadArray Reader (Illumina) to measure the signal intensity of the labeled target. Raw data were analyzed with microarray software (Bead Studio Gene Expression; version 3.4.0; Illumina) for quality control, background analysis, and normalization with the rank-invariant algorithm. Normalized data were further analyzed for comparative molecular and cellular pathway regulation using Ingenuity Pathway Analysis (P = 0.05 and Δ of 0.19; QIAGEN; Calvano et al., 2005). The microarray data are available in the NCBI Gene Expression Omnibus database under accession no. GSE78831.

Retina layer sectioning
Retina layer sectioning of fresh prepared retinas was performed according to the following steps (Fig. S2). In brief, a fresh retina was dissected, and eight evenly spaced cuts were made radially to flatten the retina before placement on a parafilm-wrapped slide. A drop of optimal cutting temperature (OCT) medium was placed on top of the retina, and then the parafilm-wrapped slide with the retina was flipped upside down, gently placed on the flat surface of a pretrimmed frozen block of OCT, and held for 1–2 min to adhere to the OCT block. The slide and parafilm were gently removed, and the flattened retina was transferred onto frozen OCT medium. OCT medium was applied to cover the flattened retina, and the frozen block with the retina was placed in a cryostat. Each horizontal retinal section was cut at 20-µm thickness, and each of ~12 sections per retina was collected into a separate RNase-free tube for RNA extraction.

Preparation of AAV2–*hRK*–*sh_c-fos* vector and AAV2
Four independent shRNAs against mouse c-fos were designed using a published algorithm (Park et al., 2008). The sequences of the mouse c-fos shRNAs are as follows. *sh_c-fos* no. 1: 5′-ACCTGGTGCTGGATTGTATCTA-3′; *sh_c-fos* no. 2: 5′-GGACCTTACCTGTTCGTGAAAC-3′; *sh_c-fos* no. 3: 5′-GGTAGTTAGTAGAGCATGTGAG-3′; *sh_Vegfa* no. 1: 5′-AACCTCACCAAAGCCAGCACAT-3′; *sh_Vegfa* no. 2: 5′-AGGACCTTGTGTGATCAGACCA-3′; *sh_Vldlr* no. 1: 5′-GGAAAGTTCAAGTGCAGAAGCG-3′; *sh_Vldlr* no. 2: 5′-GGAATGCCATATCAACGAATGC-3′; *sh_Vldlr* no. 3: 5′-GGGATCTGCAGTCAAATTTGTA-3′; and scramble shRNA control: 5′-GATTTAAGACAAGCGTATAACA-3′. The shRNAs were cloned into a CAGmiR30-GFP plasmid to test the knockdown efficiency in pup retinas and photoreceptor 661W cells. T. Li (National Eye Institute, Bethesda, MD) and C. Cepko (Harvard Medical School, Boston, MA) provided AAV constructs containing the *hRK* promoter. Recombinant AAV2 vectors were produced as previously described (Grieger et al., 2006; Vandenberghe et al., 2010). In brief, AAV vector, rep/cap packaging plasmid, and adenoviral helper plasmid were mixed with polyethylenimine (Sigma–Aldrich) and transfected into HEK293T cells (catalog no. HCL4517; Thermo Fisher Scientific). 72 h after transfection, cells were harvested, and the cell pellet was resuspended in virus buffer, followed by three cycles of freeze thaw and homogenization (Dounce). Cell debris was pelleted at 5,000 *g* for 20 min, and the supernatant was run on an iodixanol gradient. Recovered AAV vectors were washed three times with PBS using Amicon 100K columns (EMD Millipore). Real-time PCR was used to determine genome titers of the recombinant AAV. This protocol also was used to prepare a control (AAV2-shControl). Viruses were diluted to various concentrations to test infection, and a concentration of ~2 × 10^{12} genome copies/ml was used for the experiments.

Subretinal injection

Subretinal injection into P1 neonate eyes was performed as previously described (Matsuda and Cepko, 2004; Wang et al., 2014) under a dissection microscope. P1 $Vldlr^{-/-}$ or WT pups were anesthetized on ice for several minutes. The eyelid was prepared with Betadine, followed by water and then 70% ethanol using cotton swabs. A blade was used to gently cut open the eyelid. The injection needle was inserted into the eyeball through the incision until slight resistance was felt. Approximately 0.5 µl of solution containing siRNA/siControl or AAV2/control (10^{12}–10^{13} genome copies/ml) was introduced into the subretinal space using a pulled angled glass pipette controlled by a FemtoJet microinjector (Eppendorf). si_c-fos was a pool of three sequences of siRNA (cat. 4390771; Ambion), containing three siRNA sequences (siRNA nos. s66197, s66198, and s66199). The left eyes were uninjected for within-animal controls. Curved forceps were used to slowly close the eyelid. Mice were placed on a circulating water blanket for warmth. The retinas were collected at P12 for PCR assay and P16 for whole mount analysis.

Immunohistochemistry

Immunohistochemistry in retinas was performed as described previously (Chen et al., 2011a; Sun et al., 2015a,b). In brief, eyes were isolated from $Vldlr^{-/-}$ and littermate WT mice and fixed in 4% paraformaldehyde for 1 h. Dissected retinas or frozen sections were placed in cold methanol for 20 min, blocked, and permeabilized in PBS containing 5% bovine serum albumin and 0.1% Triton X-100 for 1 h. The following antibodies were used: isolectin IB_4 (121413; Invitrogen), CX3CR1 (bs-1728R; Bioss), IBA1 (019-19741; Wako Pure Chemical Industries), DAPI (D3571; Invitrogen), and SOCS3 (2923; Cell Signaling Technology). For morphological studies, mouse eyes were enucleated and fixed in 4% paraformaldehyde in PBS, cryoprotected in 30% sucrose in PBS, embedded in OCT compound (Tissue-Tek), and snap frozen. 16 µm–thick sections were taken on a cryostat (Leica Biosystems) and stained with hematoxylin and eosin (Sigma-Aldrich) followed by standard protocol.

RNA isolation and quantitative RT–PCR

Total RNA was extracted from mouse retinas using an RNeasy kit (QIAGEN) and reverse transcribed with SuperScript III reverse transcription (Thermo Fisher Scientific) to generate cDNA. Quantitative PCR was performed using a 7300 system (Applied Biosystems) with SYBR FAST qPCR kits (Kapa Biosystems) using *Rhodopsin*, *Pecam*, *Vldlr*, *CD68*, *CD11β*, *CD45*, *c-fos*, *Il6*, *Il1β*, *Tnf*, *mmp10*, *Socs3*, *uPA*, *c-jun*, *Vegf120*, *Vegf164*, and *Vegf188* primers. Primer sequences for RT-PCR were as follows. *c-fos*: 5′-AACAGATCCGAGCAG CTTCTA-3′ (forward) and 5′-TTTTGAGCTTCAACC GGCATC-3′ (reverse); *c-jun*: 5′-GTCCCCTGTCTGATT TGTAGGAA-3′ (forward) and 5′-CCACACCATCTTCTG GTGTACAGT-3′ (reverse); *Il1b*: 5′-GCCCATCCTCTG TGACTCATG-3′ (forward) and 5′-GGAGCCTGTAGT GCAGCTGTCT-3′ (reverse); *Il6*: 5′-TGGAGTCACAGA AGGAGTGGCTAAG-3′ (forward) and 5′-TCTGACCAC AGTGAGGAATGTCCAC-3′ (reverse); *Pecam1*: 5′-GAG CCCAATCACGTTTCAGTTT-3′ (forward) and 5′-TCC TTCCTGCTTCTTGCTAGCT-3′ (reverse); *Rhodopsin*: 5′-TCATGGTCTTCGGAGGATTCAC-3′ (forward) and 5′-TCACCTCCAAGTGTGGCAAAG-3′ (reverse); *Socs3*: 5′-GTTGAGCGTCAAGACCCAGT-3′ (forward) and 5′-GGGTGGCAAAGAAAAGGAG-3′ (reverse); *Tnf*: 5′-TCC AGTAGAATCCGCTCTCCT (forward) and 5′-GCCACA AGCAGGAATGAGAAG-3′ (reverse); *Tnfaip3*: 5′-ACC ATGCACCGATACACGC-3′ (forward) and 5′-AGCCAC GAGCTTCCTGACT-3′ (reverse); *uPA*: 5′-GAAGTCCTC CCTCCTTTAAATGTG-3′ (forward) and 5′-TGGGAG TTGAATGAAGCAGTGT-3′ (reverse); *Vegf120*: 5′-AAC GATGAAGCCCTGGAGTG-3′ (forward) and 5′-TGA GAGGTCTGGTTCCCGA-3′ (reverse); *Vegf164*: 5′-AAC GATGAAGCCCTGGAGTG-3′ (forward) and 5′-GAC AAACAAATGCTTTCTCCG-3′ (reverse); *Vegf188*: 5′-AACGATGAAGCCCTGGAGTG-3′ (forward) and 5′-AAC AAGGCTCACAGTGAACG-3′ (reverse); *Vegfa*: 5′-GGA GATCCTTCGAGGAGCACTT-3′ (forward) and 5′-GGC GATTTAGCAGCAGATATAAGAA-3′ (reverse); and *Vldlr*: 5′-TCTCTTGCTCTTAGTGATGG-3′ (forward) and 5′-CTTACAACTGATATTGCTGGG-3′ (reverse).

Western blotting

A standard Western blot protocol was used with minor modifications. In brief, radioimmunoprecipitation assay buffer (89900; Thermo Fisher Scientific) was used to lyse cells. Proteinase inhibitor cocktail (P8340; Sigma-Aldrich) was added. Proteins were separated by electrophoresis using 4–12% NuPAGE Novex bis-Tris gels (NP0321BOX; Invitrogen). Mouse β-actin (A1978; Sigma-Aldrich) antibody was used for control.

Preparation of lenti–*Socs3* vector and virus

Mouse *Socs3* cDNA was inserted into plentiCMV/TO (775-1) with CMV promoter using a Gateway LR clonase kit (Invitrogen) according to the manufacturer's instruction, and sequences were confirmed by sequencing at the Boston Children's Hospital Intellectual and Developmental Disabilities Research Center Molecular Genetics Core Facility. *Socs3*-carrying lentiviruses were produced as follows. In brief, *Lenti-Socs3* or lenti-control, REV, VSVG, and pMDL (gas-pol) packaging plasmids were mixed with polyethylenimine and transfected into HEK293T cells (cat. no. HCL4517; Thermo Fisher Scientific). 72 h after transfection, the cell medium was harvested, and cellular debris was removed by centrifugation at 1,500 rpm before filtration over a 0.22-µm low-protein binding filter. Then, the filtered medium was centrifuged using a SW28 rotor (37 ml) for 2 h at 19,500 rpm (50,000 g) at 4°C. The supernatant was removed, and 100 ml PBS was added to the pellet and transferred to a new tube after 5–10 min. The virus was aliquotted and stored at −80°C.

Electroretinography (ERG)

Retinal function was assessed by ERG as previously described (Zhang et al., 2013) in 3-mo untreated WT mice and littermate $Vldlr^{-/-}$ mice treated with AAV-hRK–shRNA targeting c-fos or $Vegfa$ or AAV-hRK–sh_control. In brief, dark-adapted, anesthetized (ketamine/xylazine) mouse pupils were dilated (Cyclomydril; Alcon), and their corneas were anesthetized (proparacaine). A Burian–Allen bipolar electrode designed for the mouse eye (Hansen Laboratories) was placed on the cornea, and the ground electrode was placed on a foot. The stimuli consisted of a series of green LED flashes of doubling intensity from ~0.0064–2.05 cd.s.m^{-2} and then white xenon arc flashes from ~8.2–1,050 cd.s.m^{-2}. The equivalent light for the green and white stimuli was determined from the shift of the stimulus/response curves. ERG stimuli were delivered using a Colordome Ganzfeld stimulator (Diagnosys LLC). The saturating sensitivity of the rod photoresponse was estimated by fitting a model of the biochemical processes involved in the activation of phototransduction to the ERG a-waves (Lamb and Pugh, 1992; Pugh and Lamb, 1993; Hood and Birch, 1994).

Photoreceptor (661W) cell culture

Cone photoreceptor cells (al-Ubaidi et al., 1992; Tan et al., 2004) were cultured as monolayers at 37°C and 5% CO_2 in a humidified atmosphere in DMEM with FBS 10% supplemented with 20 µg/500 ml hydrocortisone (H-2270; Sigma-Aldrich), 20 µg/500 ml progesterone (P-8783; Sigma-Aldrich), 0.016 g/500 ml putrescine (P-7505; Sigma-Aldrich), and 20 µl/500 ml β-mercaptoethanol (M-6250; Sigma-Aldrich). No mycoplasma contamination of the cells was detected. An equal number of 661W cells (3×10^5) was plated in each well of 6-well dishes. Cells were treated with $AAV2$-hRK-$sh\_control$ or $AAV2$-hRK–sh_Vldlr for overnight. On day 2, the cell medium was changed and treated with $AAV2$-hRK-$sh\_control$ or $AAV2$-hRK–sh_c-fos for overnight. On day 3, the medium was changed with fresh culture medium. After 48 h, photoreceptors were collected to determine gene expression by real time PCR.

Statistics

Results are presented as mean ± SEM and were compared using two-tailed unpaired Student's t test. Statistical analyses were performed with Prism (v5.0; GraphPad Software). A p-value <0.05 was considered to be statistically significant.

Online supplemental material

Fig. S1 shows there was no macrophage recruitment in P12 $Vldlr^{-/-}$ retinas. Fig. S2 shows a diagram of retinal layer sectioning. Fig. S3 shows knocking down c-fos reduced neovascularization in $Vldlr^{-/-}$ retinas. Fig. S4 shows the mRNA expression of c-Jun and uPA in WT and $Vldlr^{-/-}$ mice and the mRNA expression of c-fos in dark-adapted $Vldlr^{-/-}$ retinas. Fig. S5 shows the body weight of mice treated with a high dose of SR11302 or control from P5 to P15. Table S1 is included as an Excel file and shows upstream regulator prediction of the microarray data.

REFERENCES

Aikawa, Y., K. Morimoto, T. Yamamoto, H. Chaki, A. Hashiramoto, H. Narita, S. Hirono, and S. Shiozawa. 2008. Treatment of arthritis with a selective inhibitor of c-Fos/activator protein-1. *Nat. Biotechnol.* 26:817–823. http://dx.doi.org/10.1038/nbt1412

al-Ubaidi, M.R., R.L. Font, A.B. Quiambao, M.J. Keener, G.I. Liou, P.A. Overbeek, and W. Baehr. 1992. Bilateral retinal and brain tumors in transgenic mice expressing simian virus 40 large T antigen under control of the human interphotoreceptor retinoid-binding protein promoter. *J. Cell Biol.* 119:1681–1687. http://dx.doi.org/10.1083/jcb.119.6.1681

Ambati, J., J.P. Atkinson, and B.D. Gelfand. 2013. Immunology of age-related macular degeneration. *Nat. Rev. Immunol.* 13:438–451. http://dx.doi.org/10.1038/nri3459

Ames, A. III, Y.Y. Li, E.C. Heher, and C.R. Kimble. 1992. Energy metabolism of rabbit retina as related to function: high cost of Na+ transport. *J. Neurosci.* 12:840–853.

Angel, P., and M. Karin. 1991. The role of Jun, Fos and the AP-1 complex in cell-proliferation and transformation. *Biochim. Biophys. Acta.* 1072:129–157.

Apte, R.S., J. Richter, J. Herndon, and T.A. Ferguson. 2006. Macrophages inhibit neovascularization in a murine model of age-related macular degeneration. *PLoS Med.* 3:e310. http://dx.doi.org/10.1371/journal.pmed.0030310

Balasubramanian, S.A., K. Krishna Kumar, and P.N. Baird. 2014. The role of proteases and inflammatory molecules in triggering neovascular age-related macular degeneration: basic science to clinical relevance. *Transl. Res.* 164:179–192. http://dx.doi.org/10.1016/j.trsl.2014.04.005

Calvano, S.E., W. Xiao, D.R. Richards, R.M. Felciano, H.V. Baker, R.J. Cho, R.O. Chen, B.H. Brownstein, J.P. Cobb, S.K. Tschoeke, et al. Inflamm and Host Response to Injury Large Scale Collab. Res. Program. 2005. A network-based analysis of systemic inflammation in humans. *Nature.* 437:1032–1037. http://dx.doi.org/10.1038/nature03985

Catar, R., J. Witowski, P. Wagner, I. Annett Schramm, E. Kawka, A. Philippe, D. Dragun, and A. Jörres. 2013. The proto-oncogene c-Fos transcriptionally regulates VEGF production during peritoneal inflammation. *Kidney Int.* 84:1119–1128. http://dx.doi.org/10.1038/ki.2013.217

Chen, J., A. Stahl, N.M. Krah, M.R. Seaward, R.J. Dennison, P. Sapieha, J. Hua, C.J. Hatton, A.M. Juan, C.M. Aderman, et al. 2011a. Wnt signaling mediates pathological vascular growth in proliferative retinopathy. *Circulation.* 124:1871–1881. http://dx.doi.org/10.1161/CIRCULATIONAHA.111.040337

Chen, M., J.V. Forrester, and H. Xu. 2011b. Dysregulation in retinal para-inflammation and age-related retinal degeneration in CCL2 or CCR2 deficient mice. *PLoS One.* 6:e22818. http://dx.doi.org/10.1371/journal.pone.0022818

Chen, Y., Y. Hu, G. Moiseyev, K.K. Zhou, D. Chen, and J.X. Ma. 2009. Photoreceptor degeneration and retinal inflammation induced by very low-density lipoprotein receptor deficiency. *Microvasc. Res.* 78:119–127. http://dx.doi.org/10.1016/j.mvr.2009.02.005

Chinenov, Y., and T.K. Kerppola. 2001. Close encounters of many kinds: Fos-Jun interactions that mediate transcription regulatory specificity. *Oncogene.* 20:2438–2452. http://dx.doi.org/10.1038/sj.onc.1204385

Combadière, C., C. Feumi, W. Raoul, N. Keller, M. Rodéro, A. Pézard, S. Lavalette, M. Houssier, L. Jonet, E. Picard, et al. 2007. CX3CR1-dependent subretinal microglia cell accumulation is associated with cardinal features of age-related macular degeneration. *J. Clin. Invest.* 117:2920–2928. http://dx.doi.org/10.1172/JCI31692

Curran, T., and B.R. Franza Jr. 1988. Fos and Jun: the AP-1 connection. *Cell.* 55:395–397. http://dx.doi.org/10.1016/0092-8674(88)90024-4

da Silva, C.G., P. Studer, M. Skroch, J. Mahiou, D.C. Minussi, C.R. Peterson, S.W. Wilson, V.I. Patel, A. Ma, E. Csizmadia, and C. Ferran. 2013. A20 promotes liver regeneration by decreasing SOCS3 expression to enhance IL-6/STAT3 proliferative signals. *Hepatology.* 57:2014–2025. http://dx.doi.org/10.1002/hep.26197

Dorrell, M.I., E. Aguilar, R. Jacobson, O. Yanes, R. Gariano, J. Heckenlively, E. Banin, G.A. Ramirez, M. Gasmi, A. Bird, et al. 2009. Antioxidant or neurotrophic factor treatment preserves function in a mouse model of neovascularization-associated oxidative stress. *J. Clin. Invest.* 119:611–623. http://dx.doi.org/10.1172/JCI35977

Dumler, I., T. Petri, and W.D. Schleuning. 1994. Induction of *c-fos* gene expression by urokinase-type plasminogen activator in human ovarian cancer cells. *FEBS Lett.* 343:103–106. http://dx.doi.org/10.1016/0014-5793(94)80298-X

Espinosa-Heidmann, D.G., I.J. Suner, E.P. Hernandez, D. Monroy, K.G. Csaky, and S.W. Cousins. 2003. Macrophage depletion diminishes lesion size and severity in experimental choroidal neovascularization. *Invest. Ophthalmol. Vis. Sci.* 44:3586–3592. http://dx.doi.org/10.1167/iovs.03-0038

Fanjul, A., M.I. Dawson, P.D. Hobbs, L. Jong, J.F. Cameron, E. Harlev, G. Graupner, X.P. Lu, and M. Pfahl. 1994. A new class of retinoids with selective inhibition of AP-1 inhibits proliferation. *Nature.* 372:107–111. http://dx.doi.org/10.1038/372107a0

Grieger, J.C., V.W. Choi, and R.J. Samulski. 2006. Production and characterization of adeno-associated viral vectors. *Nat. Protoc.* 1:1412–1428. http://dx.doi.org/10.1038/nprot.2006.207

Hafezi, F., J.P. Steinbach, A. Marti, K. Munz, Z.Q. Wang, E.F. Wagner, A. Aguzzi, and C.E. Remé. 1997. The absence of *c-fos* prevents light-induced apoptotic cell death of photoreceptors in retinal degeneration in vivo. *Nat. Med.* 3:346–349. http://dx.doi.org/10.1038/nm0397-346

Halazonetis, T.D., K. Georgopoulos, M.E. Greenberg, and P. Leder. 1988. c-Jun dimerizes with itself and with c-Fos, forming complexes of different DNA binding affinities. *Cell.* 55:917–924. http://dx.doi.org/10.1016/0092-8674(88)90147-X

Heckenlively, J.R., N.L. Hawes, M. Friedlander, S. Nusinowitz, R. Hurd, M. Davisson, and B. Chang. 2003. Mouse model of subretinal neovascularization with choroidal anastomosis. *Retina.* 23:518–522. http://dx.doi.org/10.1097/00006982-200308000-00012

Hoffman, G.E., M.S. Smith, and J.G. Verbalis. 1993. c-Fos and related immediate early gene products as markers of activity in neuroendocrine systems. *Front. Neuroendocrinol.* 14:173–213. http://dx.doi.org/10.1006/frne.1993.1006

Hood, D.C., and D.G. Birch. 1994. Rod phototransduction in retinitis pigmentosa: estimation and interpretation of parameters derived from the rod a-wave. *Invest. Ophthalmol. Vis. Sci.* 35:2948–2961.

Joyal, J.S., Y. Sun, M.L. Gantner, Z. Shao, L.P. Evans, N. Saba, T. Fredrick, S. Burnim, J.S. Kim, G. Patel, et al. 2016. Retinal lipid and glucose metabolism dictates angiogenesis through the lipid sensor Ffar1. *Nat. Med.* 22:439–445. http://dx.doi.org/10.1038/nm.4059

Khani, S.C., B.S. Pawlyk, O.V. Bulgakov, E. Kasperek, J.E. Young, M. Adamian, X. Sun, A.J. Smith, R.R. Ali, and T. Li. 2007. AAV-mediated expression targeting of rod and cone photoreceptors with a human rhodopsin kinase promoter. *Invest. Ophthalmol. Vis. Sci.* 48:3954–3961. http://dx.doi.org/10.1167/iovs.07-0257

Klein, R., B.E. Klein, S.E. Moss, T.Y. Wong, L. Hubbard, K.J. Cruickshanks, and M. Palta. 2004. The relation of retinal vessel caliber to the incidence and progression of diabetic retinopathy: XIX: the Wisconsin epidemiologic study of diabetic retinopathy. *Arch. Ophthalmol.* 122:76–83. http://dx.doi.org/10.1001/archopht.122.1.76

Kueng-Hitz, N., C. Grimm, N. Lansel, F. Hafezi, L. He, D.A. Fox, C.E. Remé, G. Niemeyer, and A. Wenzel. 2000. The retina of *c-fos*−/− mice: electrophysiologic, morphologic and biochemical aspects. *Invest. Ophthalmol. Vis. Sci.* 41:909–916.

Lamb, T.D., and E.N. Pugh Jr. 1992. A quantitative account of the activation steps involved in phototransduction in amphibian photoreceptors. *J. Physiol.* 449:719–758. http://dx.doi.org/10.1113/jphysiol.1992.sp019111

Lee, Y.N., J. Tuckerman, H. Nechushtan, G. Schutz, E. Razin, and P. Angel. 2004. c-Fos as a regulator of degranulation and cytokine production in FcεRI-activated mast cells. *J. Immunol.* 173:2571–2577. http://dx.doi.org/10.4049/jimmunol.173.4.2571

Li, C., Z. Huang, R. Kingsley, X. Zhou, F. Li, D.W. Parke II, and W. Cao. 2007. Biochemical alterations in the retinas of very low-density lipoprotein receptor knockout mice: an animal model of retinal angiomatous proliferation. *Arch. Ophthalmol.* 125:795–803. http://dx.doi.org/10.1001/archopht.125.6.795

Luo, L., H. Uehara, X. Zhang, S.K. Das, T. Olsen, D. Holt, J.M. Simonis, K. Jackman, N. Singh, T.R. Miya, et al. 2013. Photoreceptor avascular privilege is shielded by soluble VEGF receptor-1. *eLife.* 2:e00324. http://dx.doi.org/10.7554/eLife.00324

Margetts, P.J., M. Kolb, L. Yu, C.M. Hoff, C.J. Holmes, D.C. Anthony, and J. Gauldie. 2002. Inflammatory cytokines, angiogenesis, and fibrosis in the rat peritoneum. *Am. J. Pathol.* 160:2285–2294. http://dx.doi.org/10.1016/S0002-9440(10)61176-5

Masli, S., and J.L. Vega. 2011. Ocular immune privilege sites. *Methods Mol. Biol.* 677:449–458. http://dx.doi.org/10.1007/978-1-60761-869-0_28

Matsuda, T., and C.L. Cepko. 2004. Electroporation and RNA interference in the rodent retina in vivo and in vitro. *Proc. Natl. Acad. Sci. USA.* 101:16–22. http://dx.doi.org/10.1073/pnas.2235688100

McKay, S., M.M. Bromhaar, J.C. de Jongste, H.C. Hoogsteden, P.R. Saxena, and H.S. Sharma. 2001. Pro-inflammatory cytokines induce c-fos expression followed by IL-6 release in human airway smooth muscle cells. *Mediators Inflamm.* 10:135–142. http://dx.doi.org/10.1080/09629350124155

Medzhitov, R. 2008. Origin and physiological roles of inflammation. *Nature.* 454:428–435. http://dx.doi.org/10.1038/nature07201

Nir, I., and N. Agarwal. 1993. Diurnal expression of c-fos in the mouse retina. *Brain Res. Mol. Brain Res.* 19:47–54. http://dx.doi.org/10.1016/0169-328X(93)90147-H

Ohki, K., K. Yoshida, T. Harada, M. Takamura, H. Matsuda, and J. Imaki. 1996. *c-fos* gene expression in postnatal rat retinas with light/dark cycle. *Vision Res.* 36:1883–1886. http://dx.doi.org/10.1016/0042-6989(95)00284-7

Park, Y.K., S.M. Park, Y.C. Choi, D. Lee, M. Won, and Y.J. Kim. 2008. AsiDesigner: exon-based siRNA design server considering alternative splicing. *Nucleic Acids Res.* 36:W97–W103. http://dx.doi.org/10.1093/nar/gkn280

Pepper, M.S. 2001. Role of the matrix metalloproteinase and plasminogen activator-plasmin systems in angiogenesis. *Arterioscler. Thromb. Vasc. Biol.* 21:1104–1117. http://dx.doi.org/10.1161/hq0701.093685

Perez, V.L., and R.R. Caspi. 2015. Immune mechanisms in inflammatory and degenerative eye disease. *Trends Immunol.* 36:354–363. http://dx.doi.org/10.1016/j.it.2015.04.003

Pugh, E.N. Jr., and T.D. Lamb. 1993. Amplification and kinetics of the activation steps in phototransduction. *Biochim. Biophys. Acta.* 1141:111–149. http://dx.doi.org/10.1016/0005-2728(93)90038-H

Rakic, J.M., V. Lambert, C. Munaut, K. Bajou, K. Peyrollier, M.L. Alvarez-Gonzalez, P. Carmeliet, J.M. Foidart, and A. Noël. 2003. Mice without uPA, tPA, or plasminogen genes are resistant to experimental choroidal neovascularization. *Invest. Ophthalmol. Vis. Sci.* 44:1732–1739. http://dx.doi.org/10.1167/iovs.02-0809

Ray, N., M. Kuwahara, Y. Takada, K. Maruyama, T. Kawaguchi, H. Tsubone, H. Ishikawa, and K. Matsuo. 2006. c-Fos suppresses systemic inflammatory response to endotoxin. *Int. Immunol.* 18:671–677. http://dx.doi.org/10.1093/intimm/dxl004

Roh, M.I., H.S. Kim, J.H. Song, J.B. Lim, H.J. Koh, and O.W. Kwon. 2009. Concentration of cytokines in the aqueous humor of patients with naive, recurrent and regressed CNV associated with amd after bevacizumab treatment. *Retina.* 29:523–529. http://dx.doi.org/10.1097/IAE.0b013e318195cb15

Roychoudhury, J., J.M. Herndon, J. Yin, R.S. Apte, and T.A. Ferguson. 2010. Targeting immune privilege to prevent pathogenic neovascularization. *Invest. Ophthalmol. Vis. Sci.* 51:3560–3566. http://dx.doi.org/10.1167/iovs.09-3890

Sakurai, E., A. Anand, B.K. Ambati, N. van Rooijen, and J. Ambati. 2003. Macrophage depletion inhibits experimental choroidal neovascularization. *Invest. Ophthalmol. Vis. Sci.* 44:3578–3585. http://dx.doi.org/10.1167/iovs.03-0097

Shiozawa, S., and K. Tsumiyama. 2009. Pathogenesis of rheumatoid arthritis and c-Fos/AP-1. *Cell Cycle.* 8:1539–1543. http://dx.doi.org/10.4161/cc.8.10.8411

Stahl, A., K.M. Connor, P. Sapieha, K.L. Willett, N.M. Krah, R.J. Dennison, J. Chen, K.I. Guerin, and L.E. Smith. 2009. Computer-aided quantification of retinal neovascularization. *Angiogenesis.* 12:297–301. http://dx.doi.org/10.1007/s10456-009-9155-3

Streilein, J.W. 1995. Immunological non-responsiveness and acquisition of tolerance in relation to immune privilege in the eye. *Eye (Lond.).* 9:236–240. http://dx.doi.org/10.1038/eye.1995.46

Streilein, J.W., K. Ohta, J.S. Mo, and A.W. Taylor. 2002. Ocular immune privilege and the impact of intraocular inflammation. *DNA Cell Biol.* 21:453–459. http://dx.doi.org/10.1089/10445490260099746

Sun, Y., M. Ju, Z. Lin, T.W. Fredrick, L.P. Evans, K.T. Tian, N.J. Saba, P.C. Morss, W.T. Pu, J. Chen, et al. 2015a. SOCS3 in retinal neurons and glial cells suppresses VEGF signaling to prevent pathological neovascular growth. *Sci. Signal.* 8:ra94. http://dx.doi.org/10.1126/scisignal.aaa8695

Sun, Y., C.H. Liu, J.P. SanGiovanni, L.P. Evans, K.T. Tian, B. Zhang, A. Stahl, W.T. Pu, T.M. Kamenecka, L.A. Solt, and J. Chen. 2015b. Nuclear receptor RORα regulates pathologic retinal angiogenesis by modulating SOCS3-dependent inflammation. *Proc. Natl. Acad. Sci. USA.* 112:10401–10406. http://dx.doi.org/10.1073/pnas.1504387112

Sung, H.J., J.I. Han, J.W. Lee, K.B. Uhm, and K. Heo. 2012. TCCR/WSX-1 is a novel angiogenic factor in age-related macular degeneration. *Mol. Vis.* 18:234–240.

Tan, E., X.Q. Ding, A. Saadi, N. Agarwal, M.I. Naash, and M.R. Al-Ubaidi. 2004. Expression of cone-photoreceptor-specific antigens in a cell line derived from retinal tumors in transgenic mice. *Invest. Ophthalmol. Vis. Sci.* 45:764–768. http://dx.doi.org/10.1167/iovs.03-1114

Usui, Y., P.D. Westenskow, T. Kurihara, E. Aguilar, S. Sakimoto, L.P. Paris, C. Wittgrove, D. Feitelberg, M.S. Friedlander, S.K. Moreno, et al. 2015. Neurovascular crosstalk between interneurons and capillaries is required for vision. *J. Clin. Invest.* 125:2335–2346. http://dx.doi.org/10.1172/JCI80297

Vandenberghe, L.H., R. Xiao, M. Lock, J. Lin, M. Korn, and J.M. Wilson. 2010. Efficient serotype-dependent release of functional vector into the culture medium during adeno-associated virus manufacturing. *Hum. Gene Ther.* 21:1251–1257. http://dx.doi.org/10.1089/hum.2010.107

Velazquez, F.N., C.G. Prucca, O. Etienne, D.S. D'Astolfo, D.C. Silvestre, F.D. Boussin, and B.L. Caputto. 2015. Brain development is impaired in c-fos−/− mice. *Oncotarget.* 6:16883–16901. http://dx.doi.org/10.18632/oncotarget.4527

Wagner, E.F., and R. Eferl. 2005. Fos/AP-1 proteins in bone and the immune system. *Immunol. Rev.* 208:126–140. http://dx.doi.org/10.1111/j.0105-2896.2005.00332.x

Wang, S., C. Sengel, M.M. Emerson, and C.L. Cepko. 2014. A gene regulatory network controls the binary fate decision of rod and bipolar cells in the vertebrate retina. *Dev. Cell.* 30:513–527. http://dx.doi.org/10.1016/j.devcel.2014.07.018

Webb, D.J., K.S. Thomas, and S.L. Gonias. 2001. Plasminogen activator inhibitor 1 functions as a urokinase response modifier at the level of cell signaling and thereby promotes MCF-7 cell growth. *J. Cell Biol.* 152:741–752. http://dx.doi.org/10.1083/jcb.152.4.741

Wei, D., X. Le, L. Zheng, L. Wang, J.A. Frey, A.C. Gao, Z. Peng, S. Huang, H.Q. Xiong, J.L. Abbruzzese, and K. Xie. 2003. Stat3 activation regulates the expression of vascular endothelial growth factor and human pancreatic cancer angiogenesis and metastasis. *Oncogene.* 22:319–329. http://dx.doi.org/10.1038/sj.onc.1206122

Wei, X., G. Wang, W. Li, X. Hu, Q. Huang, K. Xu, W. Lou, J. Wu, C. Liang, Q. Lou, et al. 2014. Activation of the JAK-STAT3 pathway is associated with the growth of colorectal carcinoma cells. *Oncol. Rep.* 31:335–341. http://dx.doi.org/10.3892/or.2013.2858

Xu, H., M. Chen, A. Manivannan, N. Lois, and J.V. Forrester. 2008. Age-dependent accumulation of lipofuscin in perivascular and subretinal microglia in experimental mice. *Aging Cell.* 7:58–68. http://dx.doi.org/10.1111/j.1474-9726.2007.00351.x

Yoshida, K., K. Kawamura, and J. Imaki. 1993. Differential expression of c-fos mRNA in rat retinal cells: regulation by light/dark cycle. *Neuron.* 10:1049–1054. http://dx.doi.org/10.1016/0896-6273(93)90053-T

Zhang, N., T.L. Favazza, A.M. Baglieri, I.Y. Benador, E.R. Noonan, A.B. Fulton, R.M. Hansen, P.M. Iuvone, and J.D. Akula. 2013. The rat with oxygen-induced retinopathy is myopic with low retinal dopamine. *Invest. Ophthalmol. Vis. Sci.* 54:8275–8284. http://dx.doi.org/10.1167/iovs.13-12544